Electronic structure changes during the on-surface synthesis of nitrogen-doped chevron-shaped graphene nanoribbons

Friedrich Maaß,[1] Manuel Utecht,[2] Stephan Stremlau,[1] Marie Gille,[3] Jutta Schwarz,[3] Stefan Hecht,[3] Tillmann Klamroth,[2] and Petra Tegeder[1,*]

[1]*Ruprecht-Karls-Universität Heidelberg, Physikalisch-Chemisches Institut, Im Neuenheimer Feld 253, 69120 Heidelberg, Germany*

[2]*Universität Potsdam, Institut für Chemie, Theoretische Chemie, Karl-Liebknecht-Straße 24-25, 14476 Potsdam, Germany*

[3]*Humboldt-Universität zu Berlin, Department of Chemistry, Brook-Taylor-Straße 2, 12489 Berlin, Germany*

Utilizing suitable precursor molecules, a thermally activated and surface-assisted synthesis results in the formation of defect-free graphene nanoribbons (GNRs), which exhibit electronic properties that are not present in extended graphene. Most importantly, they have a band gap in the order of a few electron volts, depending on the nanoribbon width. In this study, we investigate the electronic structure changes during the formation of GNRs, nitrogen-doped (singly and doubly N-doped) as well as non-N-doped chevron-shaped CGNRs on Au(111). Thus we determine the optical gaps of the precursor molecules, the intermediate nonaromatic polymers, and finally the aromatic GNRs, using high-resolution electron energy loss spectroscopy and density functional theory calculations. As expected, we find no influence of N-doping on the size of the optical gaps. The gap of the precursor molecules is around 4.5 eV. Polymerization leads to a reduction of the gap to a value of 3.2 eV due to elongation and thus enhanced delocalization. The CGNRs exhibit a band gap of 2.8 eV, thus the gap is further reduced in the nanoribbons, since they exhibit an extended delocalized π-electron system.

I. INTRODUCTION

Graphene nanoribbons (GNRs) consist of quasi-one-dimensional structures that exhibit tunable electronic and magnetic properties. These properties depend on their width and edge symmetry [1–9]. For instance, the band gap depends inversely on the GNR width. Conventional top-down approaches for GNR fabrication, such as lithography [7,10] or unzipping of carbon nanotubes [11,12], cannot provide defect-free and narrow ribbons. Instead, a bottom-up generation based on an on-surface synthesis has been proven to result in defect-free GNRs with nanometer-scale widths and atomically precise edge structures. Thereby, the GNR formation occurs on a noble metal surface [Au(111) or Ag(111)] via a thermally activated and surface-assisted two-step reaction involving a polymerization of a specific precursor molecule followed by cyclodehydrogenation [4,13,14]. Following this approach, various armchair-edged GNR (AGNR) structures [4,8,15], B-[16,17] and S-doped [18] AGNRs, AGNR heterostructures [3,5,6], and chevron-shaped GNRs (CGNR), including substitutional doping with zero [4,19], one [19], two [19,20], and four [5] nitrogen atoms per precursor molecule as well as, very recently, a zigzag edge topology, have been generated [21]. In the majority of cases, the experimental analysis of both the GNR formation and the electronic properties (e.g., transport levels and gaps) scanning tunneling microscopy (STM) and scanning tunneling spectroscopy (STS) have been used. In some cases, photoemission [19,22–28], inverse photoemission [24], high-resolution electron energy loss spectroscopy (HREELS) [19,22], and optical spectroscopy [29] have also been utilized.

The electronic structure of the chevron-type GNR and its N-doped derivatives (see Fig. 1) on Au(111) have been studied recently [19,27]. It has been demonstrated that the size of the band gap of the nanoribbons is independent of the degree of nitrogen doping, whereas the valence and conduction bands shift linearly down in energy by approximately 0.1 eV per N atom [19]. However, here we examine the electronic structure changes *during* the formation of the CGNRs on Au(111), i.e., we analyze the electronic properties of the precursor molecules and the corresponding polymers using HREELS. HREELS not only enables us to follow the CGNR formation, viz. the subsequent polymerization and cyclodehydrogenation processes by analyzing the vibrational spectra [19,22], it also allows us to determine the electronic properties such as optical gaps [19,30,31]. Additionally, density functional theory (DFT) is employed to characterize the electronic states of the precursor molecules, the polymeric intermediates, and the aromatic CGNRs. We find very good agreement for the monomers and the nanoribbons with respect to the measured and calculated band gaps (optical gaps). We observe a reduction of the optical gaps when going from the monomers to the polymers to the CGNRs due to an increasing delocalization of the electron systems.

II. METHODS

The Au(111) surface was prepared by the standard procedure of ion sputtering and annealing. The molecular precursor 6,11-dibromo-1,2,3,4-tetraphenyl-triphenylene and the N-doped derivatives (see Fig. 1), respectively, were evaporated from a Knudsen cell onto the gold substrate held at 120 K (see Refs. [19,27]). Annealing the sample to 520 K led to the generation of the polymer, while at 710 K the CGNRs were formed. The precursor monomers, the polymers, and the respective CGNRs were analyzed with angle-resolved vibrational HREELS using a primary electron energy of

---

*Author to whom all correspondence should be addressed: tegeder@uni-heidelberg.de
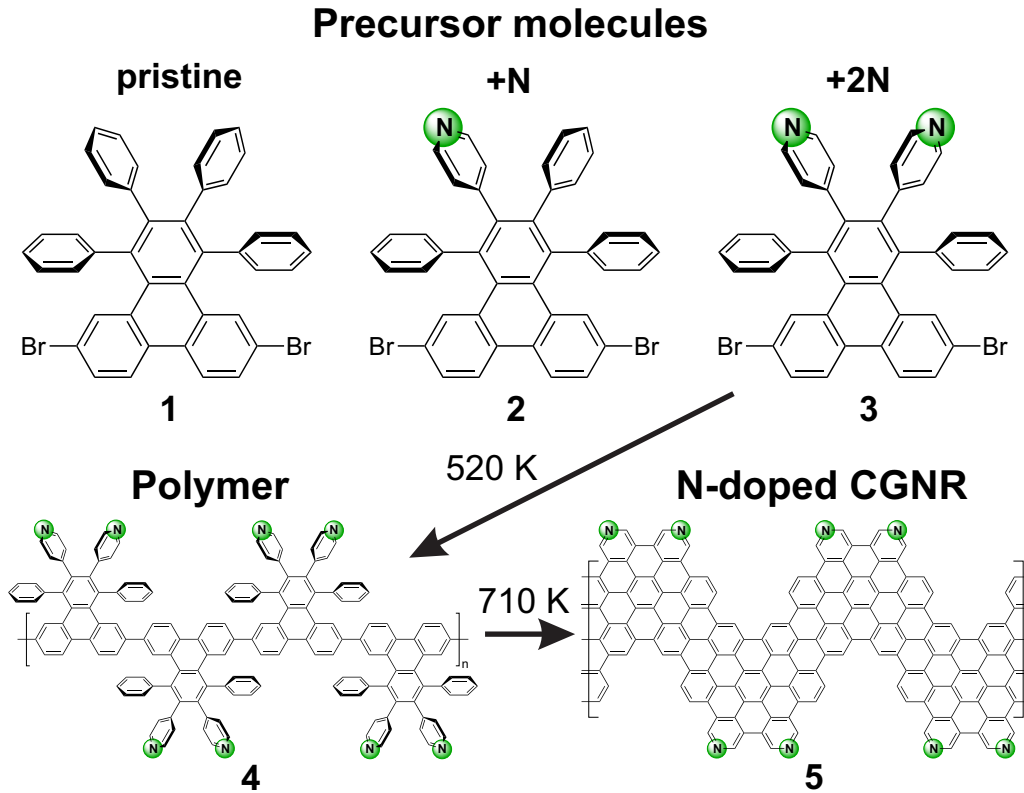
FIG. 1. Precursor molecules (1–3) for the generation of chevron-shaped graphene nanoribbons (CGNRs) with defined N-doping via on-surface polymerization followed by cyclodehydrogenation. Shown are monomers with either zero (pristine), one (+N), or two (+2N) N atoms, while the synthesis is exemplified for the case of doubly N-doped CGNR.

4.5 eV. To gain insight into the electronic structure, electronic HREELS was utilized. Thereby, the electron energy was set to 15.5 eV. The energy resolution measured as the full width at half-maximum (FWHM) of the elastically scattered electrons (elastic peak) was around 28 cm^{-1} in the case of the vibrational spectra and around 64 cm^{-1} for the electronic spectra (for experimental details, see Refs. [31,32]). To estimate the CGNR coverage, temperature-programmed desorption experiments on co-adsorbed Xe were used. A coverage of approximately 2/3 of a monolayer was determined. While our experimental methods do not enable us to determine the length of the CGNR, STM measurements have shown that the typical length at least for the undoped CGNR is in the order of tens of nanometers [4].

For the DFT calculations we used the PBE0 [33] hybrid functional as implemented in the GAUSSIAN09 program package [34] together with the 6-311G** basis set for the monomers, as was done in Ref. [25]. For the computationally more demanding periodic calculations, a 6-31G* basis set was employed. Test calculations gave only small differences for the smaller basis set. For instance, we get only a difference of ≈0.05 eV in the band gap for the pristine polymer and less than 0.01 eV for the pristine CGNR if we compare the results for the 6-31G* basis set with those for the 6-311G** basis set. For the periodic calculations, the same parameters are used as in Ref. [25], i.e., 120 k-points in the first Brillouin zone and a cutoff of 600 bohr in real space. All structures were fully optimized if not stated otherwise. The optimized structures of the monomer as well as the unit cells of the polymer and of

the CGNR in the case of doping with two N-atoms (+2N) are shown in Fig. 2.

Several isomers for the polymer and the nanoribbon exist in the case of doping with one N atom. If two monomers are used to build the polymer structure, one obtains four possible compositional "isomers" for the polymer and the CGNR. The unit cell of the polymer contains four N atoms, "NNNN," in the +2N case, which are shown as blue atoms in Fig. 2(b). Two of these four N atoms, "NNNN," need to be exchanged by carbon atoms to obtain the +1N case. As only one N atom is contained in one monomer unit, we end up with the possibilities of a "NCNC" isomer (equal to "CNCN") and a "NCCN" isomer (equal to "CNNC"). For similar reasons, we get a "NNCC" isomer (equal to "CCNN") and a "NCNC" isomer (equal to "CNCN") in the case of the CGNR, because here the unit cell is chosen differently. If one considers larger polymer repeats, more combinations would be possible. However, we expect small effects, because we also get only small differences for the two possible cases described here (see below).

III. RESULTS

The thermally activated and surface-assisted formation steps from the precursor molecules to the polymer and finally to the CGNRs on Au(111) can be followed nicely by angle-resolved vibrational HREELS because well-defined and pronounced changes in the vibrational structure are observed for each step. Figure 3 exemplifies the data for the singly
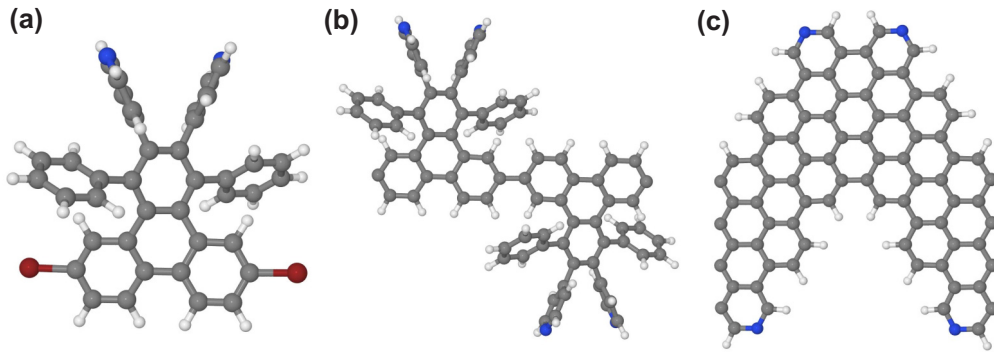
FIG. 2. Shown are the optimized structures of the monomer (a), the unit cells of the polymer (b), and the CGNR (c) in the case of doping with two N atoms (+2N). The calculations for the monomer were done at the PBE0/6-311G** level of theory, while the periodic calculations were done at the PBE0/6-31G* level of theory (for details, see the text). Carbon atoms are colored gray, hydrogen atoms white, nitrogen atoms blue, and bromine atoms red.

doped (+N) polymer and the corresponding aromatic CGNR. Note that the results for the pristine (undoped) [19] and doubly doped (+2N) species are similar.

For the linear polymer on Au(111), we observe several out-of-plane molecular vibrations, namely the phenyl-ring torsion mode [$\tau(C-C)$] at 695 cm^{-1}, and the C–H bending modes [$\gamma(C-H)$] at 767, 839, and 963 cm^{-1}. In addition, in-plane modes are also clearly visible, such as C–H bending modes [$\delta(C-H)$] at 1063 and 1156 cm^{-1}, the C–C stretch vibrations [$\nu(C=C)$] at 1304 and 1428 cm^{-1}, as well as a C–C

FIG. 3. Changes in the vibrational HREELS data observed during the cyclodehydrogenation reaction step from the singly doped (+N) polymer to the corresponding nanoribbon (+1N-CGNR) recorded with a primary electron energy of 4.5 eV in specular and 7° off-specular scattering geometry.

bending mode [$\delta(C-C)$] at 1589 cm^{-1}. The C–H stretching vibration $\nu(C-H)$ at 3048 cm^{-1} is very pronounced. Heating up the polymer phase in order to form the CGNR via cyclodehydrogenation leads to significant changes in the vibrational signature, as can be seen in Fig. 3(b). The number of molecular vibrations found in the spectrum is reduced to two modes: the out-of-plane modes, i.e., the phenyl ring torsion mode $\tau(C-C)$ at 749 cm^{-1} and the bending mode $\gamma(C-H)$ at 793 cm^{-1}, which are both dipole-active. This clearly demonstrates that all phenyl and pyridine rings are orientated parallel to the surface, i.e., they adopt a flat-lying geometry, as expected for the aromatic CGNR.

Electronic HREELS is employed to gain insights into the electronic structure changes during the on-surface synthesis of the CGNRs, viz., we studied the monomers, polymers, as well as the nanoribbons. Figure 4 shows the results for the nine investigated adsorbate/substrate systems. In the case of the monomers, we measured multilayers adsorbed on Au(111), thus the influence of the metallic substrate on the electronic states is negligible, while the polymers and CGNRs are in direct contact with the Au(111) surface. The peaks we observe correspond to intramolecular electronic transitions (e.g., HOMO-LUMO transitions), i.e., they are associated with optical gaps. The values for the electronic transitions (determined at the peak maxima) are summarized in Table I.

As expected, no influence of N-doping on the size of the optical gaps for all species (monomers and CGNRs) is observed [19]. The introduction of nitrogen atoms into the π-backbone stabilizes the frontier orbitals (and increases the electron affinity), while the size of the HOMO (VB)-LUMO (CB) gap is nearly unaffected. For the monomers, the HOMO-LUMO gap is around 4.5 eV. The higher-lying transition around 7.1 eV (for the 1N-CGNR at 6.3 eV) may be attributed to transitions between lower-lying occupied molecular states (HOMO-n) to the LUMO or higher-lying unoccupied states (LUMO+m). Note that the intensity ratios between the HOMO-LUMO transition and the higher-lying transition change due to N-doping, i.e., with increasing doping the intensity of the HOMO-LUMO transition rises. The scattering cross section seems to be affected by N-doping. From the polymer-covered surface, the electron energy loss intensities are very low. We observe a transition around
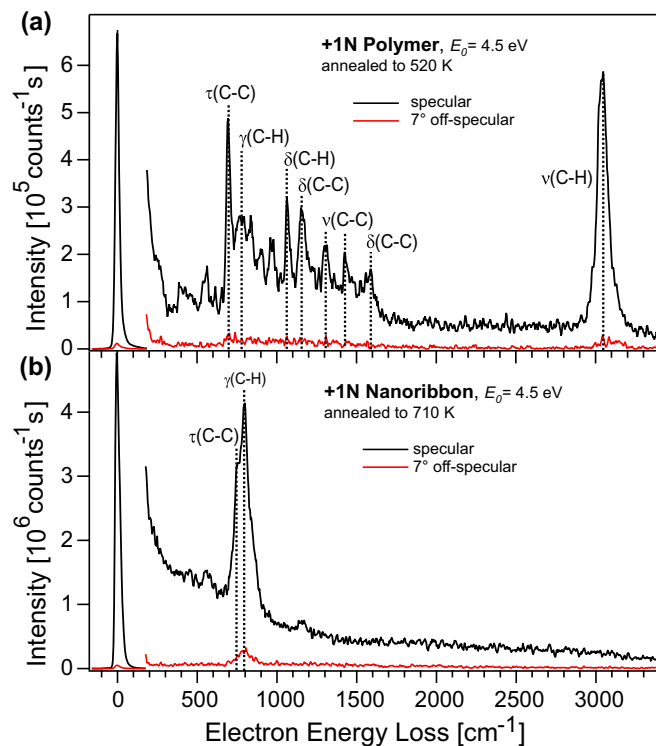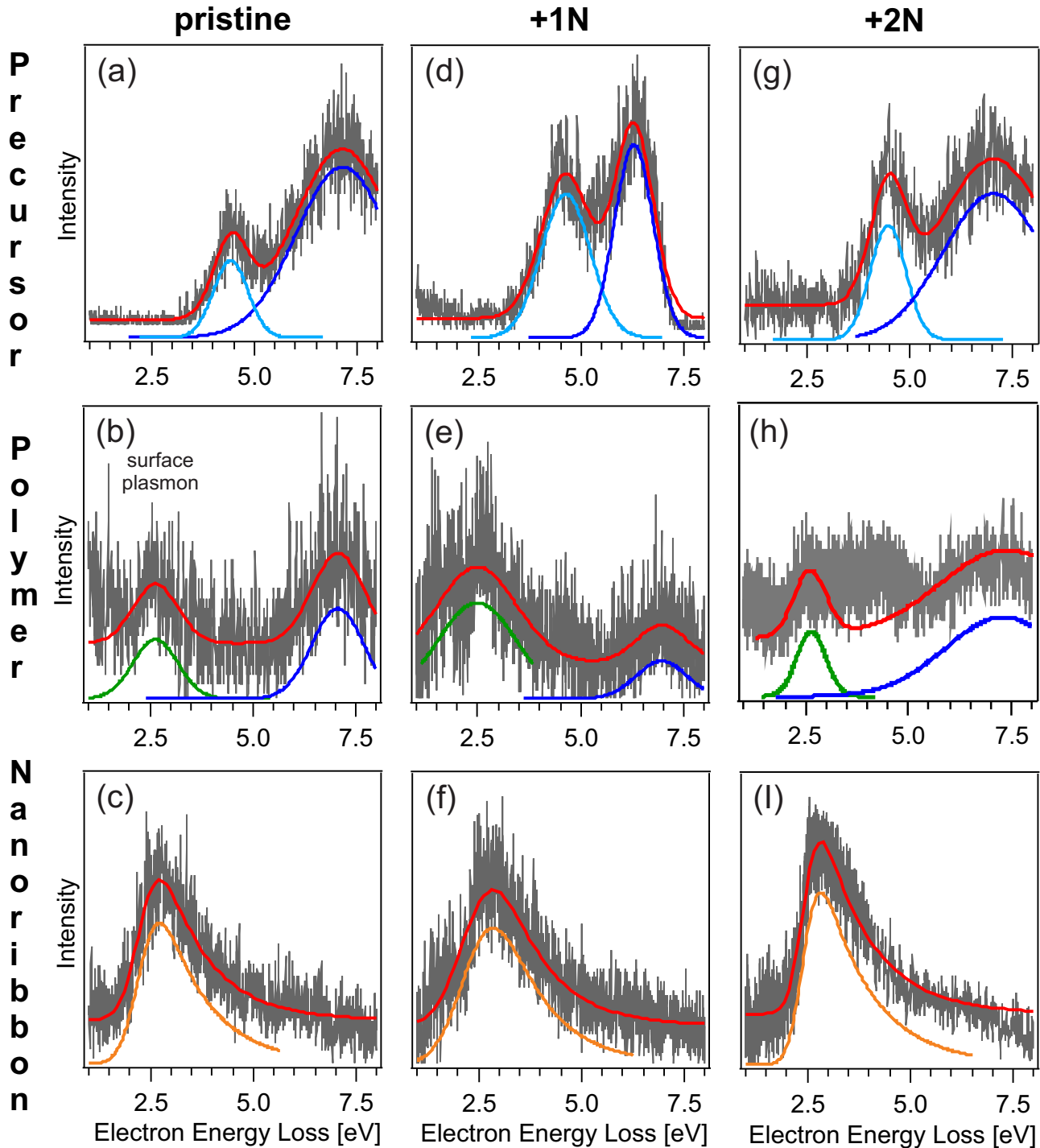
FIG. 4. Electronic structure changes during the on-surface synthesis of chevron-shaped graphene nanoribbons on Au(111). (a)–(c) Electronic HREEL data of the nondoped (pristine) compounds, (d)–(f) the corresponding spectra for the singly doped, and (g)–(i) for the doubly N-doped derivatives.

2.5 eV, which can be assigned to Au(111) surface plasmon [35]. In addition, higher-lying electronic transitions around 7.1 eV exhibit the same energetic position as in the monomer. Most likely the involved electronic states are located at the terminal phenyl or pyridine rings, which are not involved in the polymerization. However, a transition associated with the optical gap is not seen due to strong interaction of the polymer backbone with the metallic substrate, as found

for other systems [36]. In the CGNRs, the electron energy loss intensities are higher compared to the polymer/Au(111) system. The transition at 7.1 eV is no longer observed, a further hint toward the involvement of the terminal phenyl or pyridine rings, because the cyclodehydrogenation drastically changes the structure of these moieties. In contrast to the polymer phases, we now observe a transition at 2.8 eV for all CGNRs due to the formation of an extended delocalized π-electron

TABLE I. Measured electronic transitions (at the peak maximum) of the three precursor molecules (multilayer regime), the corresponding polymers, and CGNRs in electron volts (eV). The errors of the energy values are ±0.05 eV for the precursor molecules and ±0.1 eV for the polymers and nanoribbons. An asterisk indicates that the transition observed at 2.5 eV is assigned to the surface plasmon of the Au(111) surface [35]. Calculated values: For the resulting polymers and nanoribbons (GNR), the minimal band gaps are given (always a direct gap at the Γ point); for the precursor monomers, the HOMO-LUMO gap are given. For the polymer in the +1N case, two values are given: one for the "NCCN" isomer, and in parentheses the value for the "NCNC" isomer. For the +1N case of the GNR, the first value corresponds to the "NCCN" isomer, while the one in parentheses is for the "NNCC" isomer (for details, see Sec. II). All values are in eV; the monomer calculations are done at the PBE0/6-311G** level, and the periodic ones are done with PBE0/6-31G*.

	Experimental values			Calculated values		
	Pristine	+1N	+2N	Pristine	+1N	+2N
Precursor	4.42 / 7.14	4.63 / 6.28	4.48 / 7.04	4.59	4.56	4.55
Polymer	2.5* / 7.1	2.5* / 7.0	2.5* / 7.1	3.44	3.42(3.73)	3.42
Nanoribbon	2.8	2.8	2.8	2.72	2.72 (2.71)	2.72

system. Thus, the transition is attributed to the band gap of the nanoribbons.

The calculated HOMO-LUMO gaps for the monomers, and band gaps for the polymers and CGNRs, are given in Table I. As we expected, N-doping does not have much of an influence on the size of the optical gaps. We observe a small lowering of the orbital energies as an effect of doping. For instance, we get a HOMO energy of −6.22 eV for the pristine compound, −6.33 eV for the +1N molecule, and −6.45 eV for the +2N molecule in the case of the monomers. Note that a similar lowering of the valence-band energy by ∼0.1 eV per N atom in the CGNRs has been found experimentally [19]. However, as one can see, the gap is much less affected. If we compare with experiment, we find that the values for the monomers and the CGNRs compare very well with the experimental data. The calculated value for the polymer phases is around 3.4 eV. Since this value is for the gas phase optimized structure, we computed band gaps for "more planar" conformations of the polymer to account for the influence of the gold substrate on the structure of the polymer. For the monomers and

the CGNRs, we do not face this problem, because (i) the monomers are measured in multilayer and (ii) the CGNRs are planar.

We changed the configuration of the polymer for the pristine compound by varying the dihedral angles determining the orientation of the terminal phenyl rings, while keeping all other internal degrees of freedom fixed. Figure 5(a) shows the optimized unit cell viewed along the polymer axis, where all these dihedral angles have different optimized values. In Fig. 5(b), all dihedral angles are set to 90°, in (c) to 60°, and in (d) to 30°. As one can see, (b) is the most "nonplanar" configuration, while (a) and (c) are comparable and (d) is the most planar one. We calculate band gaps of 3.46 eV for (b), 3.44 eV for (c), and 3.24 eV for (d) compared with 3.44 eV for (a). This means we indeed get a smaller band gap for a "more planar" structure. Most likely also the backbone of the polymer is affected by the surface. To account for this, however, an atomistic model of the surface would be needed, which would require enormous computational resources on the chosen level of theory.
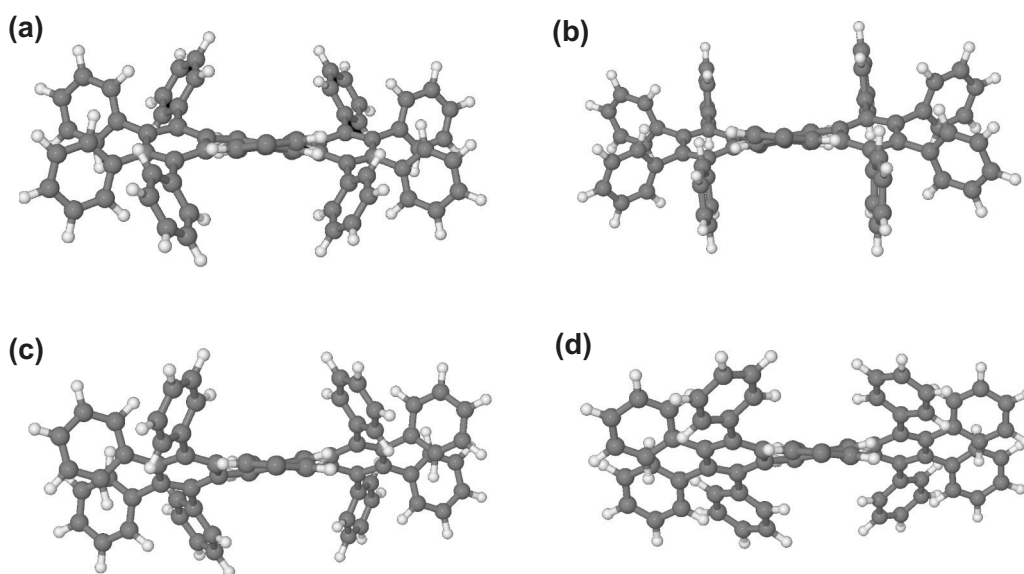
FIG. 5. Different geometries of the pristine polymer with different planarity (for details, see the text). Part (a) shows the optimized polymer, in (b) all dihedral angles determining the orientation of the terminal phenyl rings are set to 90°, in (c) these dihedral angels are set to 60°, and in (d) they are set to 30° (the same color code as in Fig. 2 is used).

Going from the monomer to the polymer, a reduction of the optical gap of around 1.3 eV is found, clearly indicating that polymerization results in an extension of the electron system. Compared to the intermediate polymer, the band gap of the CGNR as the final reaction product is reduced by 0.5 eV from 3.24 eV for the polymer to 2.72 eV in the case of the CGNR. We attribute this to the different degree of electron delocalization in the two systems. The CGNR exhibits an extended delocalized π-electron system, which resembles a two-dimensional electron gas.

IV. SUMMARY

In summary, we have utilized high-resolution electron energy loss spectroscopy (HREELS) and density functional theory (DFT) calculations to study the electronic properties of organic compounds during the on-surface synthesis of various chevron-shaped graphene nanoribbons (GNRs) on Au(111). Thereby, we investigated the electronic states of three different precursor molecules—a nondoped, a singly N-doped, and a doubled N-doped monomer—the corresponding polymer phases, and finally the GNRs. In particular, we determined the optical gaps of the precursor monomers, polymers, and nanoribbons. We found good agreement between the measured and calculated values. The monomers possess an optical gap (HOMO-LUMO transition) around 4.5 eV. The calculated value for the optical gap of the polymers is 3.2 eV. A further decrease of the band gap value of 2.8 eV has been determined for the nanoribbons. The decrease of the optical gap during the on-surface synthesis starting from the monomer going via the polymer to the nanoribbon is attributed to an increase of the extension and thus delocalization of the π-electron system.

[1] Z.-W. Son, M. L. Cohen, and S. G. Louie, Nature (London) **444**, 347 (2006).

[2] L. J. C. Tao, O. V. Yazyev, Y.-C. Chen, J. Feng, X. Zhang, R. B. Capaz, J. M. Tour, A. Zettl, S. G. Louie, H. Dai, and M. F. Crommie, Nat. Phys. **7**, 616 (2011).

[3] Y.-C. Chen, T. Cao, C. Chen, Z. Pedramrazi, D. Haberer, D. D. Oteyza, F. R. Fischer, S. G. Louie, and M. F. Crommie, Nat. Nanotechnol. **10**, 156 (2015).

[4] J. Cai, P. Ruffieux, R. Jaafar, M. Bieri, T. Braun, S. Blankenburg, M. Muoth, A. P. Seitsonen, M. Saleh, X. Feng, K. Müllen, and R. Fasel, Nature (London) **466**, 470 (2010).

[5] J. Cai, C. A. Pignedoli, L. Talirz, P. Ruffieux, H. Söde, L. Liang, V. Meunier, R. Berger, R. Li, X. Feng, K. Müllen, and R. Fasel, Nat. Nanotechnol. **9**, 896 (2014).

[6] S. Blankenburg, J. Cai, P. Ruffieux, R. Jaafar, D. Passerone, X. Feng, K. Müllen, R. Fasel, and C. Pignedoli, ACS Nano **6**, 2020 (2012).

[7] M. Y. Han, B. Özyilmaz, Y. Zhang, and P. Kim, Phys. Rev. Lett. **98**, 206805 (2007).

[8] Y. Chen, D. G. D. Oteyza, Z. Pedramrazi, C. Chen, F. R. Fischer, and M. F. Crommie, ACS Nano **7**, 6123 (2013).

[9] Y.-W. Son, M. L. Cohen, and S. G. Louie, Phys. Rev. Lett. **97**, 216803 (2006).

[10] Y. Zhang, Y.-W. Tan, H. L. Stormer, and P. Kim, Nature (London) **438**, 201 (2005).

[11] D. V. Kosynkin, A. L. Higginbotham, A. Sinitskii, J. R. Lomeda, A. Dimiev, B. K. Price, and J. M. Tour, Nature (London) **458**, 872 (2009).

[12] L. Jiao, L. Zhang, X. Wang, G. Diankov, and H. Dai, Nature (London) **458**, 877 (2009).

[13] A. Narita, X.-Y. Wang, X. Feng, and K. Müllen, Chem. Soc. Rev. **44**, 6616 (2015).

[14] L. Talirz, P. Ruffieux, and R. Fasel, Adv. Mater. **28**, 6222 (2016).

[15] H. Zhang, H. Lin, K. Sun, L. Chen, Y. Zagranyarski, N. Aghdassi, S. Duhm, Q. Li, D. Zhong, Y. Li, K. Müllen, H. Fuchs, and L. Chi, J. Am. Chem. Soc. **137**, 4022 (2015).

[16] R. R. Cloke, T. Marangoni, G. Nguyen, T. Joshi, D. J. Rizzo, C. Bronner, T. Cao, S. G. Louie, M. F. Crommie, and F. R. Fischer, J. Am. Chem. Soc. **137**, 8872 (2015).

[17] S. Kawai, S. Saito, S. Osumi, S. Yamaguchi, A. S. Foster, P. Spijker, and E. Meyer, Nat. Commun. **6**, 8098 (2015).

[18] G. D. Nguyen, F. M. Toma, Z. P. T. Cao, C. Chen, D. J. Rizzo, T. Joshi, C. Bronner, Y.-C. Chen, M. Favaro, S. G. Louie, F. R. Fischer, and M. F. Crommie, J. Phys. Chem. C **120**, 2684 (2016).

[19] C. Bronner, S. Stremlau, M. Gille, F. Brauße, A. Haase, S. Hecht, and P. Tegeder, Angew. Chem. Int. Ed. **52**, 4422 (2013).

[20] Y. Zhang, Y. Zhang, G. Li, J. Lu, X. Lin, S. Du, R. Berger, R. X. Feng, K. Müllen, and H.-J. Gao, Appl. Phys. Lett. **105**, 023101 (2014).

[21] P. Ruffieux, S. Wang, B. Yang, C. Sánchez-Sánchez, J. Liu, T. Dienel, L. Talirz, P. Shinde, C. A. Pignedoli, D. Passerone, T. Dumslaff, X. Feng, K. Müllen, and R. Fasel, Nature (London) **531**, 489 (2016).

[22] C. Bronner, F. Leyssner, S. Stremlau, M. Utecht, P. Saalfrank, T. Klamroth, and P. Tegeder, Phys. Rev. B **86**, 085444 (2012).

[23] P. Ruffieux, J. Cai, N. C. Plumb, L. Patthey, D. Prezzi, A. Ferretti, E. Molinari, X. Feng, K. Müllen, C. A. Pignedoli, and R. Fasel, ACS Nano **6**, 6930 (2012).

[24] S. Linden, D. Zhong, A. Timmer, N. Aghdassi, J. H. Franke, H. Zhang, X. Feng, K. Müllen, H. Fuchs, L. Chi, and H. Zacharias, Phys. Rev. Lett. **108**, 216801 (2012).

[25] C. Bronner, M. Utecht, A. Haase, P. Saalfrank, T. Klamroth, and P. Tegeder, J. Chem. Phys. **140**, 024701 (2014).

[26] C. Bronner, J. Björk, and P. Tegeder, J. Phys. Chem. C **119**, 486 (2015).

[27] C. Bronner, A. Haase, and P. Tegeder, Phys. Rev. B **91**, 045428 (2015).

[28] C. Bronner, D. Gerbert, A. Broska, and P. Tegeder, J. Phys. Chem. C **120**, 26168 (2016).

[29] R. Denk, M. Hohage, P. Zeppenfeld, J. Cai, C. A. Pignedoli, H. Söde, R. Fasel, X. Feng, K. Müllen, S. Wang, D. Prezzi, A. Ferretti, A. Ruini, E. Molinari, and P. Ruffieux, Nat. Commun. **5**, 4253 (2014).

[30] L. Hahn, F. Maaß, T. Bleith, U. Zschieschang, H. Wadepohl, H. Klauk, P. Tegeder, and L. H. Gade, Chem. Eur. J. **21**, 17691 (2015).

[31] F. Maass, A. Stein, B. Kohl, L. Hahn, L. H. Gade, M. Mastalerz, and P. Tegeder, J. Phys. Chem. C **120**, 2866 (2016).

[32] P. Tegeder, J. Phys.: Condens. Matter **24**, 394001 (2012).

[33] C. Adamo and V. Barone, J. Chem. Phys. **110**, 6158 (1999).

[34] M. J. Frisch, G. W. Trucks, H. B. Schlegel, *Gaussian 09 Revision D.01* (Gaussian Inc., Wallingford, 2013).

[35] S. J. Park and R. E. Palmer, Phys. Rev. Lett. **102**, 216805 (2009).

[36] V. Shklover, F. S. Tautz, R. Scholz, S. Sloboshanin, M. Sokolowski, J. A. Schaefer, and E. Umbach, Surf. Sci. **454-456**, 60 (2000).